Journal of Medicinal Chemistry

ARTICLE

pubs.acs.org/jmc

Benzimidazole Inhibitors Induce a DFG-Out Conformation of Never in Mitosis Gene A-Related Kinase 2 (Nek2) without Binding to the Back Pocket and Reveal a Nonlinear Structure−Activity Relationship†

Savade Solanki,[⊥,‡] Paolo Innocenti,[⊥,‡] Corine Mas-Droux,[⊥,§] Kathy Boxall,[‡] Caterina Barillari,[‡,§] Rob L. M. van Montfort,[‡,§] G. Wynne Aherne,[‡] Richard Bayliss,*[,§] and Swen Hoelder*[,‡]

[‡]The Institute of Cancer Research, Cancer Research UK Cancer Therapeutics Unit, 15 Cotswold Road, Sutton, Surrey SM2 5NG, United Kingdom

[§]The Institute of Cancer Research, Section of Structural Biology, Chester Beatty Laboratories, 237 Fulham Road, London SW3 6JB, United Kingdom

Supporting Information

ABSTRACT: We describe herein the structure−activity relationship (SAR) and cocrystal structures of a series of Nek2 inhibitors derived from the published polo-like kinase 1 (Plk1) inhibitor (*R*)-**1**. Our studies reveal a nonlinear SAR for Nek2 and our cocrystal structures show that compounds in this series bind to a DFG-out conformation of Nek2 without extending into the enlarged back pocket commonly found in this conformation. These observations were further investigated, and structure-based design led to Nek2 inhibitors derived from (*R*)-**1** with more than a hundred-fold selectivity against Plk1.

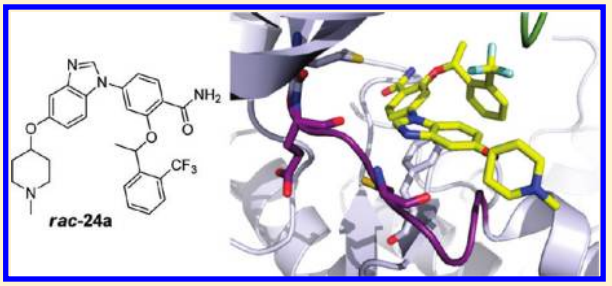

INTRODUCTION

Inducing aberrant mitosis has been explored as a cancer therapy for many decades.[1] While initial drugs predominantly targeted microtubules, more recently, nonstructural components of the mitotic machinery have been in the focus of drug discovery efforts. In particular, kinases such as Plk1 or Aurora kinases have received great attention and as a result several inhibitors have reached clinical trials.[2]

A mitotic kinase that has so far not been exploited is the serine/threonine kinase Nek2. Nek2 plays a key role in cell division: it localizes to the centrosome and regulates spindle pole organization and separation through phosphorylation of substrates including centrosomal Nek2-associated protein 1 (C-Nap1), rootletin, and ninein-like protein (Nlp).[3] In addition to its centrosomal role, Nek2 has also been implicated in chromatin condensation through phosphorylation of high mobility group AT-hook 2 (HMGA2) and spindle checkpoint control through interaction with, or phosphorylation of, highly expressed in cancer 1 (Hec1),[4] mitotic arrest deficient-like 1 (Mad1), and mitotic arrest deficient-like 2 (Mad2).[5]

Even though published studies exploring Nek2 silencing through siRNA suggest that Nek2 is a promising target,[6] so far very few inhibitors have been disclosed. Recently published benzimidazole Plk1 inhibitor (*R*)-**1** has been shown to have significant activity against Nek2 (Figure 1).[7] In addition, we have recently reported aminopyrazine **2** (Figure 1) as a potent Nek2 inhibitor.[8] As part of our efforts to develop Nek2 inhibitors, we decided to investigate if benzimidazole (*R*)-**1** could serve as starting point for improved compounds with high selectivity over Plk1. The results of these studies are presented here.

Chemistry. The thiophene series was prepared according to a previously described route.[7,9,10] Nitration of ester **3** gave nitrothiophene **4**,[11] which could be easily separated from the undesired regioisomer (Scheme 1). The benzylic ethers **5a** and **5b** were prepared by means of a Mitsunobu coupling,[12] while methyl ether **5c** was obtained by treatment with methyl iodide and potassium carbonate. Reduction of the nitro group functionality was performed with iron powder in acetic acid (**6a** and **6b**) or alternatively under high pressure hydrogenation conditions (**6c**).

Coupling with the suitable aromatic bromide according to a modified Buchwald−Hartwig procedure[9b] gave nitro derivatives **7**, which were easily reduced and cyclized in one pot under hydrogenation conditions and in the presence of methyl orthoformate to yield benzimidazoles **8**. Protected hydroxyimidazoles **8a** and **8b** were further elaborated by treatment with trifluoroacetic acid to afford alcohols **9a** and **9b**, which were coupled with 1-Boc-4-hydroxypiperidine under Mitsunobu conditions to give protected amines **10a** and **10b** (Scheme 2). Hydrogenolysis of benzyl derivative **10b** gave thiophene phenol **10c**, which was transformed into ethers **11a** and **11b** using Mitsunobu conditions or into **11c** employing potassium carbonate and methyl iodide.

Received: September 9, 2010
Published: March 02, 2011

dx.doi.org/10.1021/jm1011726 | *J. Med. Chem.* 2011, 54, 1626–1639

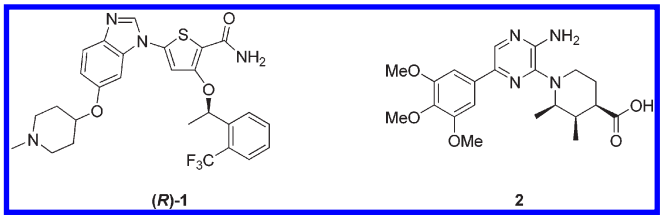

Figure 1. Structures of known Nek2 inhibitors.

Protected amines **10a**,**b** and **11** were transformed into the corresponding methyl amines using a mixture of formic acid and formaldehyde to yield thiophenes **12a**,**b** and **12e**,**f** (Scheme 2). These conditions, though, proved too harsh for benzyl ether **12d**, which was cleanly cleaved leaving thiophene phenol **12c**. Despite this setback, this material was successfully employed to reintroduce the ether functionality by means of Mitsunobu coupling affording **12d**. Finally, esters **8c**,**d**, **12a**,**b**, and **12d**−**f** were submitted to ammonolysis in methanol to yield target thiophenes ***rac*-1** and **13** (Scheme 3).

The first compound of the phenyl series was assembled by means of a Mitsunobu coupling of phenol **14**[13] to afford benzyl ether **15** (Scheme 4). Reduction of the nitro group with iron powder in acetic acid gave aniline **16**, and subsequent coupling to 4-(3-bromo-4-nitrophenoxy)-1-methylpiperidine[14] using a modified Buchwald−Hartwig reaction produced nitroderivative **17**. A one-pot reduction and cyclization under hydrogenolysis conditions yielded benzimidazole **18**, which was transformed into the target amide **19** by treatment with ammonia in methanol.

Compounds **24**[16] were prepared starting from aniline **16**, which was coupled to known 1-iodo-4-(4-methoxybenzyloxy)-2-nitrobenzene[9b] using a modified Buchwald−Hartwig reaction to produce nitroderivative **20** (Scheme 5). The reduction/cyclization reaction was performed as usual under hydrogenolytic conditions, affording benzimidazole **21**. The paramethoxybenzyl (PMB) protective group was removed using trifluoroacetic acid, and the resulting phenol **22** was coupled under Mitsunobu conditions with 1-Boc-4-hydroxypiperidine to yield protected amine **23a** or with cyclohexanol to afford ether **23b**. Amine **23d** was instead prepared by treatment of phenol **22** with cesium carbonate and 3-dimethylamino-1-propyl chloride hydrochloride. Derivatives **23c** and **23e** were also produced starting from compound **23a** by cleavage of the *tert*-butyl carbamate and subsequent reductive amination with formaldehyde or (1-ethoxycyclopropoxy)trimethylsilane, respectively. Finally, target amides **24** were prepared by ammonolysis in methanol (Scheme 5).

RESULTS AND DISCUSSION

The benzimidazole-type Plk1 inhibitor (***R*)-1** (Figure 1) was reported to inhibit Nek2 with an IC_{50} of 25 nM.[7] In our hands, the racemic mixture ***rac*-1** showed an IC_{50} of 160 nM against Nek2 (Table 1). We ascribed the 6-fold difference compared to the literature value (25 nM) to differences in the assay conditions and to the fact that we tested ***rac*-1** as the racemate. The IC_{50} of 160 nM translated into a modest ligand efficiency[17] (LE, 0.24) due to the relatively high molecular weight (545 Da). The modest efficiency of benzimidazole ***rac*-1** is not surprising given that it was optimized for Plk1 and not for Nek2.

Benzimidazoles and related heteroaromatic motifs have widely been described as kinase-targeting scaffolds that engage in hydrogen bonds with the hinge region of the kinase protein.[18] We hypothesized that trimming the substituents of the benzimidazole core of ***rac*-1** should eventually lead to a smaller, fragment-like molecule with reduced potency against Nek2 but significantly improved LE. This smaller but more ligand efficient molecule would serve as a starting point for the design of selective Nek2 inhibitors. This hypothesis was based on the published observations[19] that low molecular weight, fragment-type inhibitors based on hinge binding motifs frequently show better LE than the fully decorated inhibitors. This should be particularly relevant if the substitution pattern was optimized for a different kinase.

Removal of the methyl piperidine substituent (**13f**, Table 1) led to a sharp decrease in the Nek2 activity and importantly to an even less ligand efficient inhibitor. One explanation for this result is that the basic piperidine group engages in a strong interaction with Nek2 that is reinforced by the observation that related Plk1 inhibitors without a suitably placed basic group did not show Nek2 cross reactivity.[18h] Next, the benzyl substituent was replaced with a methyl group (**13d**), again resulting in substantial loss of activity and concomitant drop in LE.

To complete the initial set of experiments, an additional benzimidazole compound was prepared in which both substituents were removed (**13e**). Interestingly, this compound showed activity comparable to the monosubstituted derivatives **13f** and **13d** and an improved LE compared to ***rac*-1**, **13f**, and **13d**. Despite this, the LE of **13e** is still modest (0.29) given its low molecular weight.[20]

These preliminary results suggest that neither of the two substituents is capable of improving Nek2 activity of the fragment compound **13e** on their own but that they act together in a cooperative manner to improve the IC_{50} more than three-hundred-fold. This is also reflected in the LE trend: undecorated benzimidazole **13e** has the best LE, which substantially drops if either of the two substituents is introduced (Table 1). Interestingly, LE significantly improves if both substituents are present to give ***rac*-1** compared with **13f** and **13d**. These results thus represent an example of nonlinear SAR around this series of inhibitors, and it is interesting to speculate whether ***rac*-1** would have been identified in a classical fragment approach starting from **13e**.

To further understand the SAR around ***rac*-1**, we next removed the substituents of the benzyl group. Again, a nonlinear relationship was observed. Removing either the benzylic methyl group (**13c**) or the trifluoromethyl group (**13b**) caused a pronounced loss of both activity and LE. When both substituents were removed, resulting in benzimidazole **13a**, the effect on Nek2 inhibition was again comparable to removing them individually (**13b** and **13c**). Finally, a comparison between compounds **13a** and **13d** showed that introduction of only the phenyl group caused a 12-fold increase in activity.

As this series of compounds was inspired by Plk1 inhibitors,[7] we decided to counter screen compounds ***rac*-1** and **13** against Plk1 to test whether a similar nonlinear effect was observed. In agreement with published data[7,10] and in contrast to the SAR observed for Nek2, the basic group was not important for high potency against Plk1 (compounds ***rac*-1** and **13f**, Table 1) even though the exact IC_{50} values of ***rac*-1** and **13f** could not be determined as they were beyond the dynamic range of our Plk1 assay. For this reason, it was also difficult to fully assess the importance of the methyl and the trifluoromethyl substituents. In agreement with data disclosed for a similar compound,[7] the trifluoromethyl group on the aromatic ring causes a significant increase (at least 5-fold, compounds ***rac*-1** and **13b**) in Plk1

Scheme 1. Synthesis of Thiophene Series I[a]

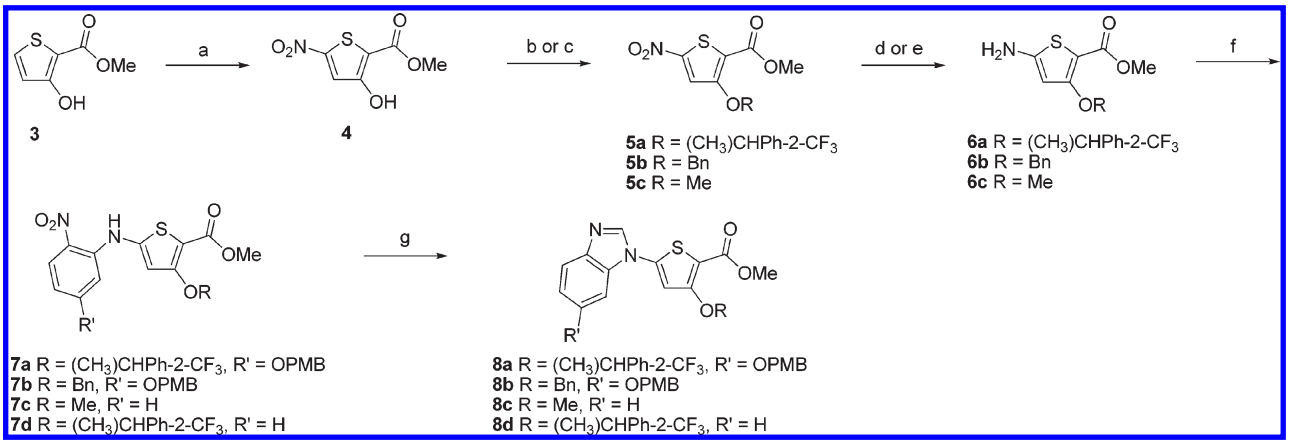

[a] Reagents and conditions: (a) HNO_3, H_2SO_4, −10 to 0 °C; (b) ROH, di-*tert*-butyl azodicarboxylate, PPh_3, DCM, 0 °C to rt (**5a** and **5b**); (c) MeI, K_2CO_3, DMF, rt (**5c**); (d) Fe, AcOH, 65 °C (**6a** and **6b**); (e) H_2, Pt(sulfided)/C 5%, 40 psi, MeOH/H_2O (95/5), 35 °C (**6c**); (f) ArBr, Cs_2CO_3, $Pd_2(dba)_3$, XANTPHOS, 1,4-dioxane, 50−70 °C; (g) H_2, Pt(sulfided)/C 5%, PPTS, $CH(OMe)_3$, EtOAc, rt.

Scheme 2. Synthesis of Thiophene Series II[a]

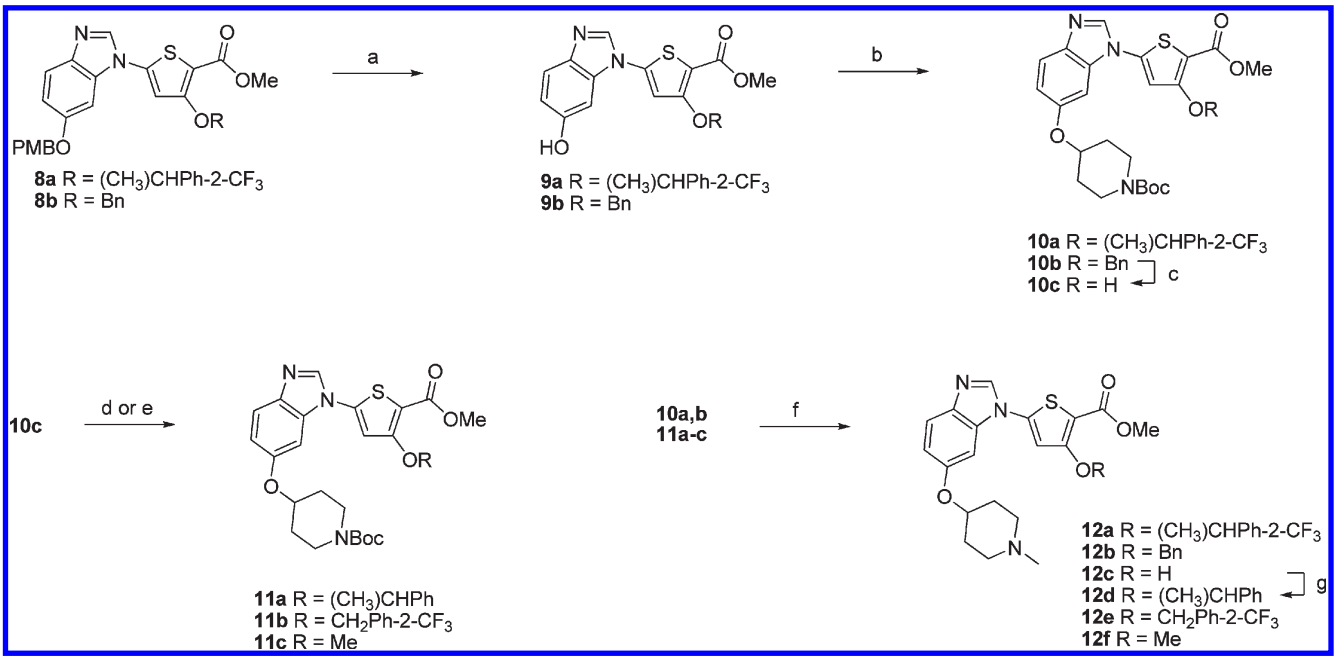

[a] Reagents and conditions: (a) TFA, DCM, 0 °C to rt; (b) 1-Boc-4-hydroxypiperidine, di-*tert*-butyl azodicarboxylate, PPh_3, DCM, 0 °C to rt; (c) H_2, Pd/C 10%, EtOH/H_2O (95/5), rt; (d) ROH, di-*tert*-butyl azodicarboxylate, PPh_3, DCM, 0 °C to rt (**11a** and **11b**); (e) MeI, K_2CO_3, DMF, rt (**11c**); (f) aq HCOH, HCOOH, 85 °C; (g) 1-phenylethanol, di-*tert*-butyl azodicarboxylate, PPh_3, DCM, 0 °C to rt.

activity. On the other hand, as evident from the Plk1 IC_{50} values of compounds **13a** and **13b**, the methyl group on its own did not significantly enhance the activity in the absence of the trifluoromethyl group. However, it is not possible to assess whether the methyl group further potentiates the effect of the trifluoromethyl group (as is does for Nek2) because the activities of compounds ***rac*-1** and **13c** were beyond the sensitivity of our Plk1 assay. The authors who initially disclosed this series of compounds encountered the same issue of assay sensitivity but noticed that the methyl group significantly improved cellular activity.[7]

Finally, it is also interesting to compare the Nek2 and Plk1 potencies of **13d** and fragment-like **13e**. Both molecules bind significantly more strongly to Plk1. Comparing the Nek2 and Plk1 activities of this series of compounds thus suggested that (1) in striking contrast with Plk1, Nek2 requires the presence of a basic group which acts in cooperative manner with the substituted phenyl group, (2) when the basic group is present, the SAR around the phenyl group is roughly parallel for Nek2 and Plk1, and (3) the significantly higher activity of ***rac*-1** for Plk1 largely stems from more potent binding of the core scaffold as evident from the IC_{50} values of **13d** and **13e**.

dx.doi.org/10.1021/jm1011726 |*J. Med. Chem.* 2011, 54, 1626–1639

Scheme 3. Synthesis of Thiophene Series III[a]

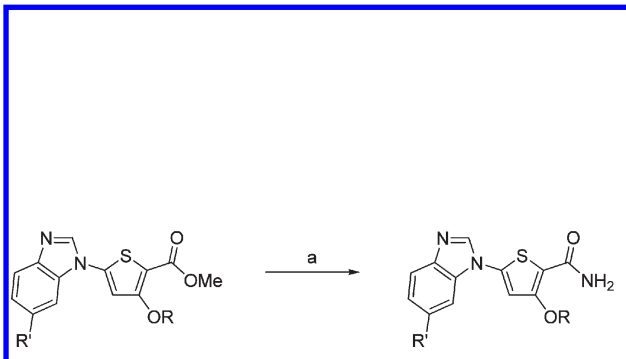

ester	amide	R	R'
12a	***rac*-1**	$(CH_3)CHPh$-2-CF_3	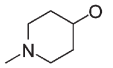
12b	**13a**	Bn	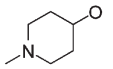
12d	**13b**	$(CH_3)CHPh$	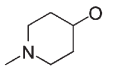
12e	**13c**	CH_2Ph-2-CF_3	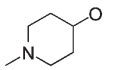
12f	**13d**	Me	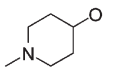
8c	**13e**	Me	H
8d	**13f**	$(CH_3)CHPh$-2-CF_3	H

[a] Reagents and conditions: (a) NH_3, MeOH, 70−75 °C.

Scheme 4. Synthesis of Compound 19[a]

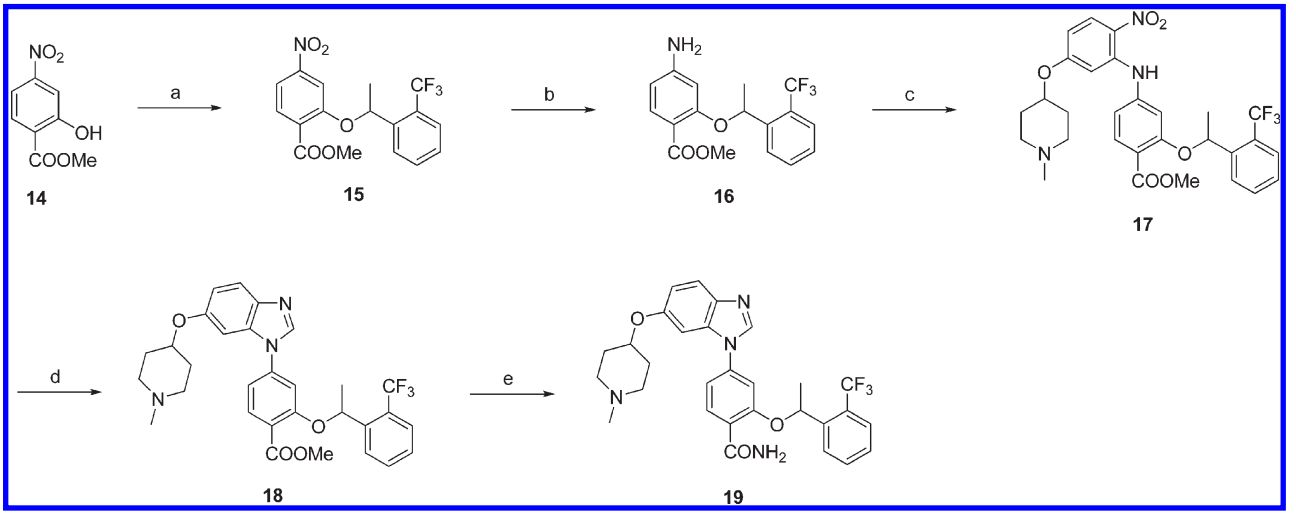

[a] Reagents and conditions: (a) 1-(2-(trifluoromethyl)phenyl)ethanol, di-*tert*-butyl azodicarboxylate, PPh_3, DCM, 0 °C to rt; (b) Fe, AcOH, 65 °C or H_2, Pd/C 10%, MeOH/H_2O, rt;[15] (c) 4-(3-bromo-4-nitrophenoxy)-1-methylpiperidine,[14] Cs_2CO_3, $Pd_2(dba)_3$, XANTPHOS, 1,4-dioxane, 60 °C; (d) H_2, Pt(sulfided)/C 5%, PPTS, $CH(OMe)_3$, EtOAc, rt; e) NH_3, MeOH, 70 °C.

To understand the observed SAR and to devise a Nek2 selective inhibitor, the crystal structure of ***rac*-1** bound to Nek2 was solved. The key interactions are shown in Figure 2. As expected the unsubstituted benzimidazole nitrogen forms a hydrogen bond with the hinge region (Cys89). The hydrogen atom attached to the benzimidazole C2 carbon is sufficiently close to Glu87 to form an aromatic hydrogen bond. The thiophene moiety is positioned between Phe148 and the gatekeeper Met86. These observations are in good agreement with the published docking pose for a similar compound in Plk1.[7] The Met86 side chain shows two conformations. The conformation that points toward the back pocket is similar to the one observed in the nucleotide-bound Nek2 structures.[21] The other conformation closer to the thiophene ring is only observed in the presence of the compound and might be induced by an attractive interaction between the sulfur atom of the gatekeeper and the aromatic ring.[22]

Because an unphosphorylated form of the kinase was crystallized, a substantial part of the activation loop (residues 167−175) was disordered. However, Asp159, Phe160, and Gly161 of the DFG motif are resolved and adopt a DFG-out conformation, which has not previously been observed in Nek2 structures. Interestingly, the structure revealed key differences between the binding mode of known DFG-out inhibitors and ***rac*-1**. The former stabilize the DFG-out conformation by placing hydrophobic groups in the enlarged back pocket of the kinase.[23] In addition, two hydrogen bonds, one to the carboxylate side chain

dx.doi.org/10.1021/jm1011726 |*J. Med. Chem.* 2011, 54, 1626–1639

Scheme 5. Synthesis of Phenyl Series[a]

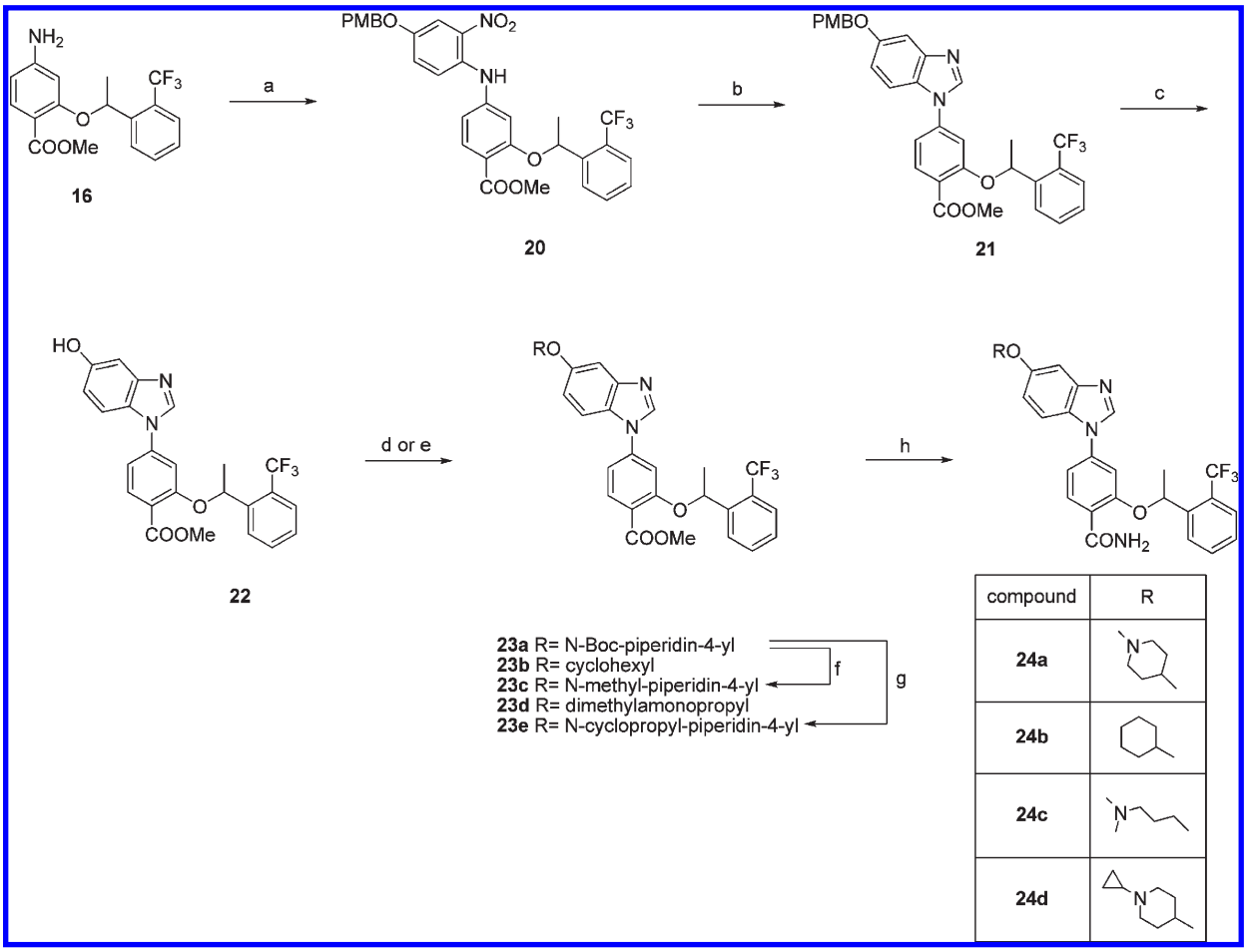

[a] Reagents and conditions: (a) 1-iodo-4-(4-methoxybenzyloxy)-2-nitrobenzene, Cs_2CO_3, $Pd_2(dba)_3$ or $Pd(dba)_2$, XANTPHOS, 1,4-dioxane, 60 °C; (b) H_2, Pt(sulfided)/C 5%, PPTS, $CH(OMe)_3$, EtOAc, rt; (c) TFA, DCM, 0 °C to rt; (d) ROH, di-*tert*-butyl azodicarboxylate, PPh_3, DCM, 0 °C to rt (**23a** and **23b**); (e) 3-dimethylamino-1-propyl chloride hydrochloride, Cs_2CO_3, DMF, rt (**23d**); (f) TFA, DCM, 0 °C then HCOH, AcOH, $NaCNBH_3$, DCM/MeOH, rt; (g) TFA, DCM, 0 °C then (1-ethoxycyclopropoxy)trimethylsilane, AcOH, $NaBH(AcO)_3$, THF, 55 °C; (h) NH3, MeOH, 70−75 °C.

of the catalytic Glu and one to the main chain nitrogen of the Asp of the DFG motif, are frequently found.[23] Compound ***rac*-1** also engages in a hydrogen bond with the NH of Asp159 of the DFG motif but does not form a hydrogen bond to the catalytic Glu, which is too far away due to a different position of the C-helix. Instead the amide group of ***rac*-1** forms an additional hydrogen bond with the backbone carbonyl group of Asp159, thereby likely stabilizing the DFG-out conformation. Crucially, ***rac*-1** does not extend into the back pocket like most DFG-out type inhibitors (Figure 2D). This binding mode of ***rac*-1** in the complex with Nek2 might be applicable to other kinases, in particular those featuring a relatively large gatekeeper (Met86 in Nek2) that can potentially block the entrance to the back pocket.

The substituted benzyl group of ***rac*-1** is well ordered with the trifluoromethyl group binding to a hydrophobic pocket formed by part of the glycine-rich loop (Ile14 and Gly15) and Cys22, which accounts for its contribution to potency (Figure 2C). Interestingly, one of the fluorine atoms is engaged in an orthogonal interaction with the carbonyl group of Ile14 (3.6 Å).[24] The phenyl ring is relatively solvent exposed, only forming a few hydrophobic interactions, e.g., with Phe148. The position of the methyl group clearly reveals the *R* configuration at the benzylic stereocenter of ***rac*-1** even though the racemic mixture ***rac*-1** was used for the soaking process, suggesting that this is the more potent enantiomer for Nek2.

As mentioned above, the benzylic methyl group increases the activity of compound ***rac*-1** about 10-fold. Although the literature suggests that an order of magnitude can be achieved by adding a methyl group if it is completely buried,[25] the crystal structure indicates that this is clearly not the case for ***rac*-1** (Figure 2C). The significant contribution of the methyl group can be understood by taking the conformation of ***rac*-1** when bound to Nek2 into account (Figure 2). To avoid the steric interaction between the methyl group and the trifluoromethyl group, analogous to $A^{1,3}$ strain,[26] the benzyl group of ***rac*-1** likely adopts a conformation in the unbound state similar to the bioactive conformation observed in the crystal structure. An analogous "cyclopropylic strain" has recently been reported for histamine H_3 receptor antagonists.[27] The contribution of the methyl group can thus at least partially be attributed to preorganizing the substituted phenyl group in which the trifluoromethyl group can interact with the hydrophobic pocket as described above. We also solved the structure of **13c**, the compound lacking the methyl group, bound to Nek2. The main difference between the cocrystal

dx.doi.org/10.1021/jm1011726 |*J. Med. Chem.* 2011, 54, 1626–1639

Table 1. Thiophene Series: Biochemical Data for Nek2 and Plk1 Assays[a]

	compound	Nek2 IC_{50} (μM)	LE	Plk1 IC_{50} (μM)	Plk1 IC_{50} / Nek2 IC_{50}
***rac*-1**	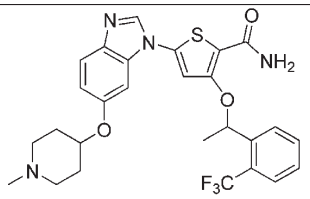	0.16 ± 0.02	0.24	< 0.009	< 0.06
13a	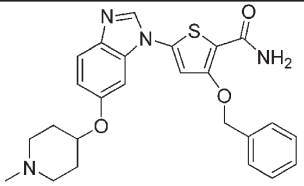	5.43 ± 1.00	0.22	0.069 ± 0.03	0.01
13b	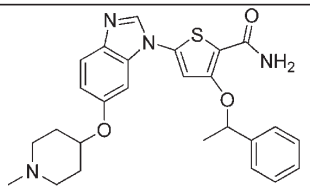	6.57 ± 1.01	0.21	0.066 ± 0.013	0.01
13c	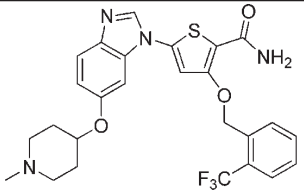	1.18 ± 0.16	0.22	< 0.009	< 0.01
13d	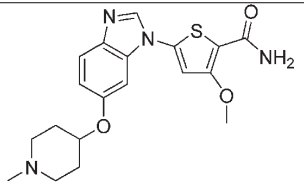	64.4 ± 5.4	0.21	1.33 (1.06, 1.60)	0.02
13e	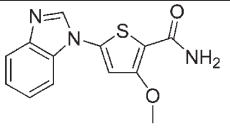	86.0	0.29	5.31 (7.59, 3.03)	0.06
13f	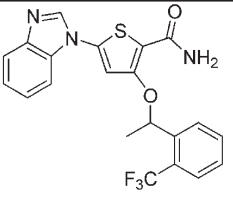	> 50	≤ 0.20	< 0.009	-

[a] Results are mean (±standard deviation (SD)) for $n \geq 3$, or mean values of two independent determinations with individual determinations in parentheses or samples run $n = 1$; compounds are racemic unless otherwise stated.

structure of ***rac*-1** and **13c** is that the substituted benzyl group is not well resolved in the case of **13c** and thus adopts different conformations (Figure 3). This observation supports the hypothesis that the methyl group contributes through conformational restriction. It is interesting to note that in the Nek2 structure bound to compound **13c**, the activation loop is more disordered (residues 161−175 are not ordered) and electron density is observed only for the backbone of Phe160. This suggests that a more constrained compound "rigidifies" the DFG motif and the N-terminal end of the activation loop.

dx.doi.org/10.1021/jm1011726 |*J. Med. Chem.* 2011, 54, 1626–1639

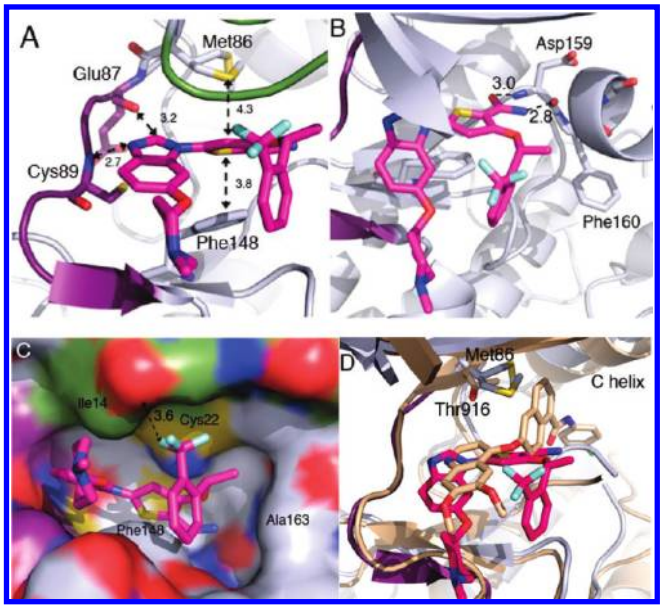

Figure 2. Binding mode of compound ***rac*-1** in the ATP pocket of Nek2. (A) Active site viewed from the entrance to show the interactions between compound ***rac*-1** and the hinge region and the packing of the thiophene group between the side chains of Met86 gatekeeper and Phe148. Met86 side chain shows two conformations. (B) Interactions between compound ***rac*-1** and the DFG motif at Asp159. (C) The surface of Nek2 is shown to illustrate the packing of the compound into the active site. The following color scheme is used for atoms: nitrogen, blue; oxygen, red; sulfur, yellow; fluorine, cyan. Compound ***rac*-1** (carbon atoms are colored magenta) and key residues within the kinase active site are shown as sticks. The hinge region carbon atoms are colored purple, and the Gly-rich loop is colored green. All distances are in Å. (D) ***rac*-1** Does not occupy the back pocket of Nek2. Overlay of Nek2 bound to ***rac*-1** (red) and kinase insert domain receptor (KDR) bound to a naphthamide inhibitor (beige, PDB 3B8Q) shows that the large Met86 gatekeeper in Nek2 hampers the access to the back pocket compared to the small Thr916 gatekeeper in KDR.

The suggested role of the methyl group and the observation that the phenyl moiety is relatively solvent exposed also explains why the latter on its own only modestly adds to activity (12 times increase, Table 1, compounds **13a** and **13d**): it primarily acts in concert with the methyl group to place the trifluoromethyl group in the correct position to fill the small hydrophobic subpocket (Figure 2).

The SAR data presented above underline the important role of the piperidine moiety. The basic group is well resolved in the crystal structure, but despite its crucial role for Nek2 activity, it does not seem to engage in any charge-assisted hydrogen bonds. However, charge−charge interactions can be long ranged and the piperidine ring is in relatively close proximity to Asp 93 (4.6 Å), potentially explaining why it contributes to activity (Figure 4).

Despite these extensive studies, neither the crystal structures nor the biological data offer a conclusive explanation for the origin of the nonlinear SAR in Nek2 observed for the compounds described. Examples of positive cooperative effects have recently been described[28] and are frequently explained by structural tightening when additional interactions are introduced,[24] making the interactions more enthalpically favorable. In this context, it is noteworthy that we also solved the cocrystal structure of **13f**, which does not have the piperidine group and is much less potent (Table 1). This structure showed that, while the benzimidazole interacts with Nek2 in a manner similar to ***rac*-1**, significantly less electron density is observed for the benzylic methyl group, suggesting that it adopts this conformation with lower occupancy compared to ***rac*-1** (Figure 3C). Like in the case of compound **13c**, in the structure of compound **13f** bound to Nek2, the DFG motif is less ordered than with compound ***rac*-1** and only the backbone of Phe160 was modeled. The DFG-out conformation is not observed in structures of apo-Nek2 or Nek2 bound to other ligands, such as ADP and ATPγS, suggesting that the DFG-out conformation is induced by ligand binding (Figure 3D). These observations are in line with the hypothesis that the cooperative SAR is caused by structural tightening. However, we can not rule out the possibility that the complex of ***rac*-1** with Nek2 is less flexible simply as a consequence of the increased potency of ***rac*-1** compared to **13c** and **13f**. The data (both in terms of quality and limiting resolution) used to determine the cocrystal structures of **13f** bound to Nek2 was slightly poorer than that used for the cocrystal structures of ***rac*-1** and **13c** (see Supporting Information, Table S1). The electron density due to the benzimidazole−thiophene core of the molecule is clear in the maps of all three structures, indicating that the data was of sufficient quality to reveal differences between the rigid core of the ligands and the flexible substituents of compounds **13c** and **13f** (Figure 3). We attempted to investigate entropy and enthalpy changes by isothermal titration calorimetry (ITC), but these experiments unfortunately did not yield interpretable data (data not shown).

Having established the SAR for Nek2 and Plk1 as well as having studied the binding mode of ***rac*-1**, we next addressed the Plk1 selectivity issue. Compound ***rac*-1** is a Plk1 inhibitor with significantly less activity against Nek2. Docking experiments (data not shown) into the Nek2 crystal structure of ***rac*-1** suggested that the thiophene ring could be replaced by a phenyl ring without interrupting the key interactions with the protein. Interestingly, several thiophene derivatives have been reported as Plk1 inhibitors whereas the corresponding phenyl compounds have not been explored to the same extent, suggesting that replacement of the thiophene by a phenyl ring could be beneficial for selectivity. Compound **19** was thus prepared and showed Nek2 activity slightly weaker than compound ***rac*-1**, but critically 20-fold less activity against Plk1 (Table 2). While this did not improve potency or LE for Nek2, it was a significant step toward a selective Nek2 inhibitor. Although the crystal structure of compound ***rac*-1** in Plk1 was not available, the fact that Plk1 shows a preference for a thiophene-based inhibitor might be explained by the difference in the gatekeeper residues, Leu in Plk1 and Met in Nek2. These amino acids strongly interact with the central aromatic moieties and may be the cause of the observed difference in recognition.

Despite the improvement in the ratio between the Nek2 and Plk1 IC_{50} values (Table 2), compound **19** still represented an approximately equipotent inhibitor of these kinases. Comparison of the crystal structure of ***rac*-1** in Nek2 with a published Plk1 crystal structure suggested a strategy to further improve selectivity: moving the basic group from the 6-position of the benzimidazole to the 5-position should lead to a clash with Arg136 of Plk1 while it should be tolerated in Nek2, which features a glycine (Gly92) at this position. This assumption was supported by published SAR data showing that substitution of the 5-position of the benzimidazole with relatively bulky substituents such as trifluoromethyl or methylsulfonyl groups led a significant drop in Plk1 activity.[10] Accordingly, compound ***rac*-24a** was prepared and gratifyingly not only showed

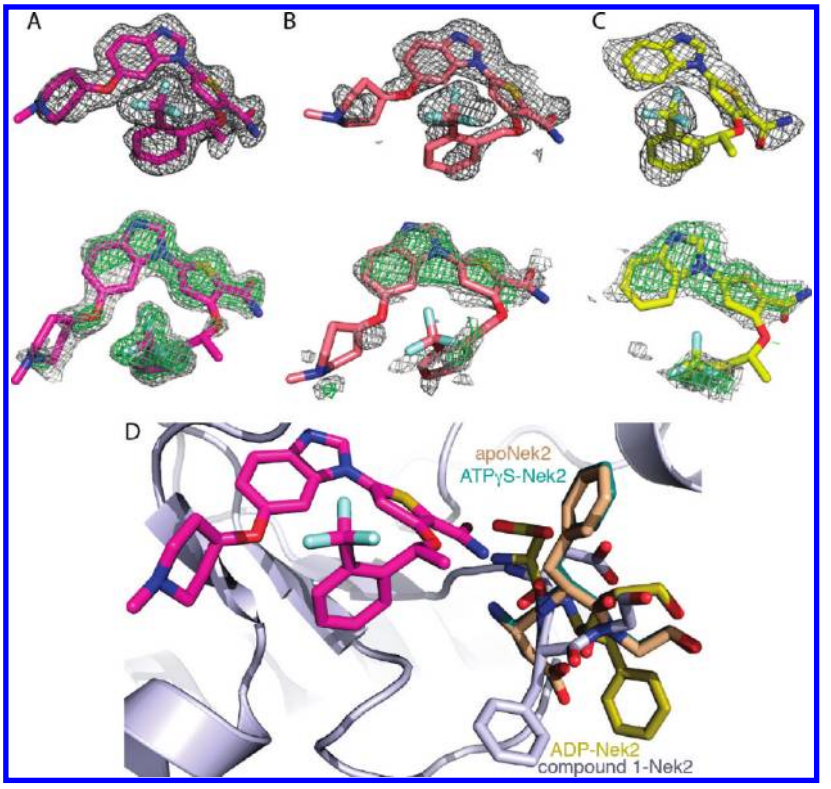

Figure 3. Structural biology data supports the structural tightening hypothesis and shows that the conformation of the activation loop of Nek2 is ligand dependent. (A−C) Upper images: final refined electron density map ($2mF_o - DF_c$) at 1 σ around compounds ***rac*-1** (2A), **13c** (2B), and **13f** (2C). Lower images: initial electron density maps generated in the absence of ligand and before refinement (gray: $2F_o - F_c$ at 1 σ, green: $F_o - F_c$ at 2.5 σ). (D) Superposition of Nek2 protein structures to show the variability in DFG motif conformation dependent on the bound ligand: apo (wheat); compound ***rac*-1** (gray), ADP (yellow), ATPγS (cyan). For clarity, regions outside the DFG motif and ligand are shown only for Nek2 bound to compound ***rac*-1**.

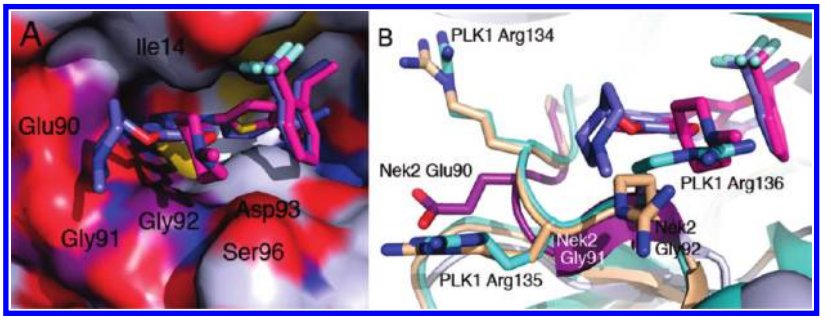

Figure 4. Structural basis of the enhanced selectivity against Plk1 achieved with compound ***rac*-24a**. (A) Comparison of the piperidine ring position for compound ***rac*-1** and ***rac*-24a** in Nek2. (B) Overlay of Nek2 structure, compounds ***rac*-1**, ***rac*-24a**, and two inhibitor-bound Plk1 structures. Residue Arg136 in Plk1 can adopt different conformations, but both will lead to a steric clash with the piperidine ring of compound ***rac*-24a**. Nek2 (carbon atoms are colored gray and purple for hinge region), Plk1 (carbon atoms are colored beige (3FC2), and green (3DB8). Carbon atoms are colored magenta in the case of ***rac*-1** and lavender in the case of ***rac*-24a**.

equipotent activity on Nek2 but negligible activity on Plk1 (Table 2).

We solved the cocrystal structure of compound ***rac*-24a** bound to Nek2. As expected, the binding modes of ***rac*-1** and ***rac*-24a** have many similarities (Figure 4). It is interesting to point out that the absolute configuration at the benzylic stereocenter of ***rac*-24a** bound to Nek2 is again *R*, as observed in the case of thiophene ***rac*-1** (Figure 4). This observation reinforces the hypothesis that the *R* configured compounds in these two series are responsible for most of the enzyme inhibition.[7] To further investigate this matter, the two enantiomers were prepared starting from optically pure benzylic alcohols and assayed for Nek2 and Plk1 inhibition. As expected, (***R*)-24a** was found to be the most active of the pair with an IC_{50} of 0.36 μM (***rac*-24a** IC_{50} = 0.57 μM) while (***S*)-24a** was shown to be a relatively weak inhibitor of Nek2 with an IC_{50} of 4.86 μM. The loss of activity of (***S*)-24a**, which is more than an order of magnitude if compared with its enantiomer, underlines the importance of the configuration at the benzylic stereocenter.

An interesting difference between the structure of thiophene ***rac*-1** and ***rac*-24a** bound to Nek2 (Figure 4) is that the piperidine ring was shifted by 4.3 Å toward the back of the catalytic pocket and was positioned above the Gly91−Gly92 residues of the hinge region. In both examples no charge-assisted hydrogen

dx.doi.org/10.1021/jm1011726 |*J. Med. Chem.* 2011, 54, 1626–1639

Table 2. Phenyl Series: Biochemical Data for Nek2 and Plk1 Assays[a]

	compound	Nek2 IC_{50} (μM)	LE	Plk1 IC_{50} (μM)	Plk1 IC_{50} / Nek2 IC_{50}
***rac*-1**	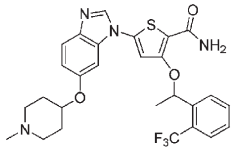	0.16 ± 0.02	0.24	< 0.009	0.06
19	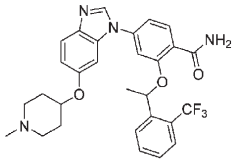	0.66 ± 0.27	0.22	0.190 (0.130, 0.250)	0.29
***rac*-24a**	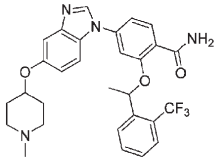	0.57 ± 0.16	0.22	87.9 (91.4, 84.4)	154
(*R*)-24a	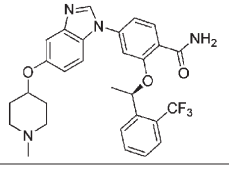	0.36 ± 0.06	0.23	51.3 (46.91, 55.62)	143
(*S*)-24a	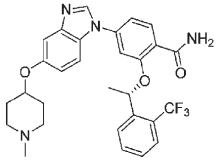	4.86 (4.11, 5.60)	0.19	inactive at 200	-
24b	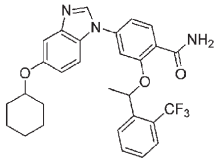	inactive at 200	-	inactive at 100	-
24c	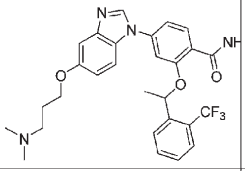	0.38 (0.43, 0.32)	0.23	15.2 (16.0, 24.4)	40
24d	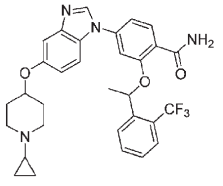	2.56 (2.36, 2.77)	0.19	inactive at 100	-

[a] Results are mean (±SD) for $n \geq 3$, or mean values of two independent determinations with individual determinations in parentheses or samples run $n = 1$; compounds are racemic unless otherwise stated.

bond can be observed, suggesting that long-range charge−charge interactions are responsible for the contributions of the piperidine ring.

To further investigate the role of this basic residue, and to elucidate the remarkable impact it has in conjunction with the presence of the fully substituted benzylic group (see Table 1,

dx.doi.org/10.1021/jm1011726 |*J. Med. Chem.* 2011, 54, 1626–1639

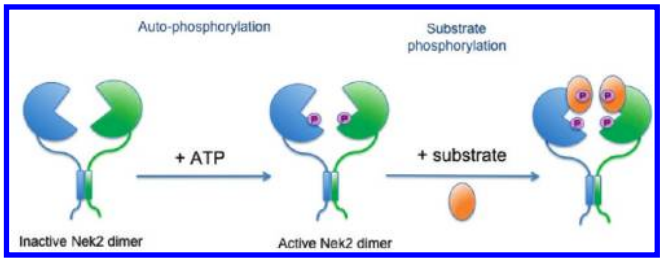

Figure 5. Auto- and substrate phosphorylation cascade: addition of ATP to the inactive Nek2 dimer initiates trans-autophosphorylation on Thr175 and activation of the protein. Active Nek2 then phosphorylates the substrate.

Table 3. Nek2 Autophosphorylation and Substrate Phosphorylation Data[a]

	compound	Nek2 auto phosphorylation IC_{50} (μM)	Nek2 substrate phosphorylation IC_{50} (μM)
***rac*-1**	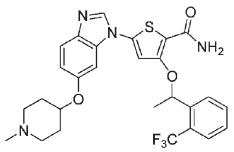	0.05 ± 0.02	0.20 (0.14, 0.26)
***rac*-24a**	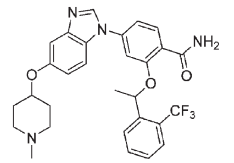	0.23 ± 0.05	0.91 (0.71, 1.11)

[a] Results are mean (±SD) for $n \geq 3$, or mean values of two independent determinations with individual determinations in parentheses; compounds are racemic unless otherwise stated.

compounds ***rac*-1** and **13f**), a few derivatives of ***rac*-24a** in which the basic group is altered were prepared (Table 2): the nonbasic cyclohexyl analogue **24b**, the open chain amine **24c**, and cyclopropylamine **24d**. While **24b** showed very weak inhibition, **24c** showed activity comparable to ***rac*-24a**, suggesting that the basic nitrogen is critical while the exact shape of the amine is not important. The crucial role of the basic nitrogen is further supported by the fact that the less basic cyclopropylamine is about 5-fold less active. Literature data[29] suggest that the pK_a of piperidine ***rac*-24a** is in the order of 9, whereas the pK_a of cyclopropylamine **24d** is around 7.5. Compound **24d** should thus be protonated to a significantly lesser degree, possibly leading to the loss in activity. Taken together, this set of data suggests that the basicity of the compounds studied here is crucial to achieve high levels of activity against Nek2 and that a charge related interaction is responsible for the contribution of the basic group.

While the crystal structures did not conclusively explain the observed nonlinear SAR, the fact that ***rac*-1** and ***rac*-24a** bind to a DFG-out conformation of Nek2 was intriguing. The DFG-out conformation is in many cases adopted by the unphosphorylated, inactive form of the kinase.[23] This is consistent with the fact that we crystallized the unphosphorylated form of the enzyme. Nek2 exists as a dimer and rapidly trans-autophosphorylates on Thr175 in the presence of ATP (Figure 5). The observation that the inhibitors described here bind to the inactive conformation suggests that they should be capable of preventing Nek2 activation through trans-autophosphorylation (Table 3). The assay used for testing the inhibitors so far employed the nonphosphorylated kinase which is preincubated with the inhibitor before autophosphorylation and subsequent substrate phosphorylation was triggered by adding ATP (Figure 5). While this assay was capable of identifying inhibitors of auto- and substrate phosphorylation, it was interesting to discern to which extent each of these events was inhibited.

To answer this question, a specific autophosphorylation assay was developed employing an antibody specific for Nek2 phosphorylated on Thr175. Interestingly, ***rac*-1** and ***rac*-24a** showed IC_{50} values of 50 and 230 nM, respectively, in this autophosphorylation assay, which is in agreement with the observation that they bind to the DFG-out conformation. To address the question of whether ***rac*-1** and ***rac*-24a** also inhibit substrate phosphorylation, the original assay conditions were slightly altered. The enzyme was first incubated with ATP to ensure complete autophosphorylation followed by incubation with the inhibitor and addition of the substrate. Under these conditions, ***rac*-1** and ***rac*-24a** showed an IC_{50} comparable to the initially employed conditions (0.20 and 0.91 μM, respectively), suggesting that these compounds can also inhibit the phosphorylated kinase. The ability of ***rac*-1** and ***rac*-24a** to inhibit Nek2 regardless of its phosphorylation state is highly desiderable.

Our results so far had identified compound **24a** as the most attractive Nek2 inhibitor in this series with good potency and selectivity versus Plk1, and we decided to further profile it. We tested ***rac*-24a** against a panel of 24 kinases. While the overall selectivity profile was reasonable (Gini coefficient for ***rac*-24a** was 0.534, see Table S2 in Supporting Information for details), a few tyrosine kinases like Abelson murine leukemia viral oncogene (Abl) or lymphocyte-specific protein tyrosine kinase (Lck) showed significant inhibition at 2 μM. Next, we tested (***R*)-24a** in our cell-based assay, which monitors centrosome splitting.[30] Disappointingly, benzimidazole (***R*)-24a** failed to have any significant effect at concentrations below 10 μM while it was found to have cytotoxic effects at higher concentrations (data not shown). We attributed the lack of activity of (***R*)-24a** in this cellular assay below 10 μM at least partially to the significantly higher ATP concentration in cells compared to the biochemical assay. The cytotoxic effects at higher concentrations can be explained by inhibition of other kinases as observed from the kinase profiling mentioned above. Finally, (***R*)-24a** showed very good permeability at physiological pH in a parallel artificial membrane permeability assay (PAMPA) (33.4×10^{-6} cm/s) and moderate metabolic degradation (see Table S3 in Supporting Information for details).

CONCLUSIONS

In summary, we designed a potent Nek2 inhibitor characterized by more than hundred-fold selectivity against Plk1 (***rac*-24a**). This and related compounds in the series showed an

unusual binding mode to the DFG-out conformation of Nek2. In addition, both ***rac*-1** and ***rac*-24a** displayed potent inhibition of substrate- and autophosphorylation. Given that very few inhibitors of Nek2 have been published so far, this represents a significant step forward. However, our data, in particular the lack of cellular activity, showed that improvement of activity and selectivity are still required. We believe that the pharmacophore defined by the cocrystal structures and SAR described here will be valuable for the identification of such improved inhibitors. A limitation for the further optimization of compound (***R*)-24a** is the still relatively moderate LE (Table 2). In this context, it is noteworthy that **13e**, which represents the core scaffold and hinge binding element of (***R*)-24a**, also shows only modest LE (Table 1). This observation suggests that exploring the pharmacophore described here with more efficient hinge binders will yield improved inhibitors with better optimization potential. Studies toward this end are underway.

Furthermore, the body of data discussed herein represents an interesting example of nonlinear SAR and is particularly relevant in the context of fragment-based approaches. Compounds **1** and **24a** might not have been identified through independent optimization of the substituents of the hinge binding fragment **13e** because the singly substituted inhibitors (compounds **13d** and **13f**, Table 1) are very weak inhibitors with poor LE. This underscores the importance of combinatorial exploration, even though chemically more demanding, in fragment optimization.

EXPERIMENTAL SECTION

General Chemistry Information. Starting materials, reagents, and solvents for reactions were reagent grade and used as purchased. Chromatography solvents were HPLC grade and were used without further purification. Thin layer chromatography (TLC) analysis was performed using Merck silica gel 60 F-254 thin layer plates. Flash column chromatography was carried out using columns prepacked with 40−63 μm silica or using standard chromatography techniques when performed on a large scale. NMR spectra were recorded on a Bruker Advance 500 MHz spectrometer, and samples were referenced to the appropriate internal nondeuterated solvent peak. In the case where a 1:1 mixture of MeOD and $CDCl_3$ was used, the samples were referenced to MeOD. The data is given as follows: chemical shift (δ) in ppm, multiplicity (where applicable), coupling constants (J) in Hz (where applicable), and integration (where applicable). LCMS analyses were performed on a Micromass LCT/Waters Alliance 2795 separations module HPLC system with a Merck Chromolith SpeedROD RP-18e 50 mm × 4.6 mm column at a temperature of 22 °C. The following solvent system, at a flow rate of 2 mL/min, was used: solvent A, methanol; solvent B, 0.1% formic acid in water. Gradient elution was as follows: 1:9 (A:B) to 9:1 (A:B) over 2.25 min, 9:1 (A:B) for 0.75 min then reversion back to 1:9 (A:B) over 0.3 min, 1:9 (A:B) for 0.2 min. Detection was with a Waters 2487 Dual λ absorbance detector (detecting at 254 nm) and ionization was electrospray (ESI). Some LCMS and all HRMS analyses were performed on a Agilent 1200 series HPLC system with a Merck Chromolith SpeedROD RP-18e 50 mm × 4.6 mm column at a temperature of 22 °C. The following solvent system, at a flow rate of 2 mL/min, was used: solvent A, methanol; solvent B, 0.1% formic acid in water. Gradient elution was as follows: 1:9 (A:B) to 9:1 (A:B) over 2.5 min, 9:1 (A:B) for 1 min then reversion back to 1:9 (A:B) over 0.3 min, 1:9 (A:B) for 0.2 min. This was connected to a Agilent 6200 time of flight (ToF) mass spectrometer (simultaneous ESI and APCI or ESI only) with detection at 254 nm. The following reference masses were used for HRMS analysis: caffeine $[M + H]^+$ = 195.087652, reserpine $[M + H]^+$ = 609.280657, and (1*H*,1*H*,3*H*-tetrafluoropentoxy)phosphazene $[M + H]^+$ = 922.009798. The purity of final compounds was determined by HPLC as described above and is ≥95% unless specified otherwise.

(±)-Methyl 4-Nitro-2-(1-(2-(trifluoromethyl)phenyl)ethoxy)benzoate (*rac*-15).

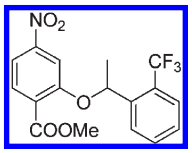

A solution of (±)-1-(2-(trifluoromethyl)phenyl)ethanol (1.03 g, 5.43 mmol), methyl 2-hydroxy-4-nitrobenzoate[13] **14** (765 mg, 3.88 mmol), and triphenylphosphine (1.43 g, 5.43 mmol) in DCM (30 mL) was cooled at 0 °C and treated with di-*tert*-butyl azodicarboxylate (1.25 g, 5.43 mmol). The mixture was allowed to reach room temperature and stirred overnight. The reaction was quenched with water and extracted with DCM. The organics were dried ($MgSO_4$), concentrated, and purified by Biotage column chromatography (0−25% EtOAc/hexane) to provide ether ***rac*-15** (1.47 g, quant). ^{1}H NMR (500 MHz, $CDCl_3$) δ 7.85 (dd, J = 8.1, 5.5 Hz, 2H), 7.79−7.67 (m, 3H), 7.56 (t, J = 7.6 Hz, 1H), 7.40 (t, J = 7.6 Hz, 1H), 5.89 (q, J = 6.2 Hz, 1H), 4.01 (s, 3H), 1.75 (d, J = 6.2 Hz, 3H).

(±)-Methyl 4-Amino-2-(1-(2-(trifluoromethyl)phenyl)ethoxy)benzoate (*rac*-16).

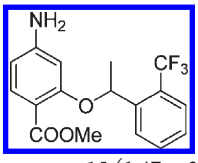

A solution of nitrobenzene ***rac*-15** (1.47 g, 3.98 mmol) in AcOH (12 mL) was heated at 65 °C for 45 min in the presence of iron powder (1.11 g, 19.88 mmol). The reaction was diluted with DCM (22 mL) and quenched with 6N NaOH (33 mL) and satd aqueous $NaHCO_3$ (10 mL). The resulting thick solution was filtrated over Celite washing with DCM and satd $NaHCO_3$. The organic phase was separated, dried ($MgSO_4$), and concentrated to afford aniline ***rac*-16** (830 mg, 62%). HRMS (ESI) m/z calcd for $C_{17}H_{17}F_3NO_3$ ($M + H$) 340.1155, found 340.1153. ^{1}H NMR (500 MHz, $CDCl_3$) δ 7.96 (d, J = 7.9 Hz, 1H), 7.71 (d, J = 8.5 Hz, 1H), 7.67−7.52 (m, 2H), 7.37 (q, J = 7.7 Hz, 1H), 6.17 (dd, J = 8.5, 2.1 Hz, 1H), 6.08 (d, J = 2.1 Hz, 1H), 5.75 (q, J = 6.1 Hz, 1H), 3.89 (s, 3H), 1.69 (d, J = 6.1 Hz, 2H).

(±)-Methyl 4-(4-(4-Methoxybenzyloxy)-2-nitrophenylamino)-2-(1-(2-(trifluoromethyl)phenyl)ethoxy)benzoate (*rac*-20).

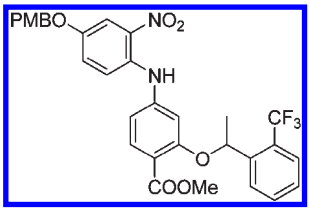

A solution of aniline ***rac*-16** (538 mg, 1.59 mmol), 1-iodo-4-(4-methoxybenzyloxy)-2-nitrobenzene[9b] (582 mg, 1.51 mmol), tris(dibenzylideneacetone)dipalladium(0) (28 mg, 0.027 mmol), XANTPHOS (46 mg, 0.08 mmol), and cesium carbonate (2.50 g, 7.67 mmol) in 1,4-dioxane (8 mL, degassed) was heated to 60 °C overnight. The mixture was filtered over Celite washing with Et_2O, the solvent removed under reduced pressure, and the residue purified by Biotage column chromatography (0−50% EtOAc/cyclohexane) to provide aniline ***rac*-20** (925 mg, quant). HRMS (ESI) m/z calcd for $C_{31}H_{28}F_3N_2O_7$ ($M + H$) 597.1843, found 597.1852. ^{1}H NMR (500 MHz, $CDCl_3$) δ 9.02 (s, 1H), 7.92 (d, J = 7.9 Hz, 1H), 7.83 (d, J = 8.4 Hz, 1H), 7.70 (t, J = 1.6 Hz, 1H), 7.65 (d, J = 7.9 Hz, 1H), 7.58 (t, J = 7.6 Hz, 1H), 7.42−7.36 (m, 3H), 7.01−6.93 (m, 4H), 6.69

(dd, J = 8.5, 2.0 Hz, 1H), 6.60 (d, J = 2.0 Hz, 1H), 5.72 (q, J = 6.1 Hz, 1H), 5.01 (s, 2H), 3.95 (s, 3H), 3.84 (s, 3H), 1.71 (d, J = 6.1 Hz, 3H).

(±)-Methyl 4-(5-(4-Methoxybenzyloxy)-1*H*-benzo[*d*]imidazol-1-yl)-2-(1-(2-(trifluoromethyl)phenyl)ethoxy)benzoate (*rac*-21).

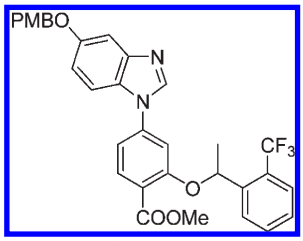

A solution of amine ***rac*-20** (925 mg, 1.55 mmol) in EtOAc (13 mL) was treated with platinum sulfided on charcoal (5% w/w, 574 mg, 0.15 mmol), PPTS (78 mg, 0.31 mmol), and methyl orthoformate (1.67 mL, 15.2 mmol). The mixture was stirred in an atmosphere of hydrogen for 20 h. The mixture was filtered over Celite washing with EtOAc, the solvent removed under reduced pressure, and the residue purified by Biotage column chromatography (0−100% EtOAc/cyclohexane) to give benzimidazole ***rac*-21** (630 mg, 71%). HRMS (ESI) m/z calcd for $C_{32}H_{28}F_3N_2O_5$ (M + H) 577.1945, found 577.1971. ^{1}H NMR (500 MHz, $CDCl_3$) δ 7.97 (d, J = 8.3 Hz, 1H), 7.93−7.90 (m, 2H), 7.69 (d, J = 7.8 Hz, 1H), 7.59 (t, J = 7.6 Hz, 1H), 7.45−7.38 (m, 3H), 7.36 (d, J = 2.3 Hz, 1H), 7.04 (dd, J = 8.3, 1.9 Hz, 1H), 6.95−6.85 (m, 5H), 5.81 (q, J = 6.1 Hz, 1H), 5.05 (s, 2H), 4.00 (s, 3H), 3.81 (s, 3H), 1.77 (d, J = 6.1 Hz, 3H).

(±)-Methyl 4-(5-Hydroxy-1*H*-benzo[*d*]imidazol-1-yl)-2-(1-(2-(trifluoromethyl)phenyl)ethoxy)benzoate (*rac*-22).

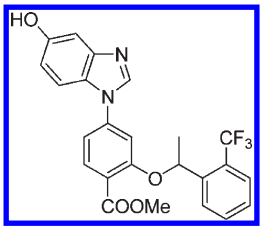

A solution of benzimidazole ***rac*-21** (630 mg, 1.09 mmol) in DCM (6 mL) was treated with trifluoroacetic acid (803 μL, 10.9 mmol) at 0 °C. The mixture was allowed to reach room temperature and stirred for 3 h. The reaction was brought to pH 5−6 with 1 M NaOH and 1 M HCl, and the aqueous layer was separated and extracted with DCM. The combined organic layers were concentrated, and the residue was purified by Biotage column chromatography (0−60% EtOAc/cyclohexane) to afford benzimidazole ***rac*-22** (470 mg, 94%). HRMS (ESI) m/z calcd for $C_{24}H_{20}F_3N_2O_4$ (M + H) 457.1370, found 457.1381. ^{1}H NMR (500 MHz, $CDCl_3$) δ 9.13 (br s, 1H), 7.96−7.89 (m, 3H), 7.66 (d, J = 7.8 Hz, 1H), 7.58 (t, J = 7.6 Hz, 1H), 7.42−7.39 (m, 2H), 7.02 (dd, J = 8.3, 1.9 Hz, 1H), 6.91 (d, J = 1.9 Hz, 1H), 6.86 (dd, J = 8.8, 2.3 Hz, 1H), 6.77 (d, J = 1.9 Hz, 1H), 5.81 (q, J = 6.1 Hz, 1H), 4.00 (s, 3H), 1.76 (d, J = 6.1 Hz, 3H).

(±)-*tert*-Butyl 4-(1-(4-(Methoxycarbonyl)-3-(1-(2-(trifluoromethyl)phenyl)ethoxy)phenyl)-1*H*-benzo[*d*]imidazol-5-yloxy)piperidine-1-carboxylate (*rac*-23a).

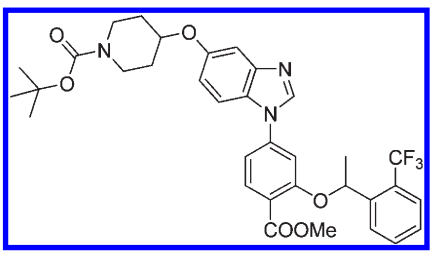

A solution of benzimidazole ***rac*-22** (146 mg, 0.32 mmol), 1-Boc-4-hydroxypiperidine (129 mg, 0.64 mmol), and triphenylphosphine (336 mg, 1.28 mmol) in DCM (2.5 mL) was cooled at 0 °C and treated with di-*tert*-butyl azodicarboxylate (147 mg, 0.64 mmol). The reaction was allowed to reach room temperature and stirred overnight. The mixture was quenched with water and extracted with DCM twice. The organics were dried (Na_2SO_4), concentrated, and purified by Biotage column chromatography (0−60% EtOAc/cyclohexane) to give benzimidazole ***rac*-23a** (205 mg, containing traces of triphenylphosphine oxide, quant). LCMS (ESI) m/z 640 (M + H). ^{1}H NMR (500 MHz, $CDCl_3$) δ 7.97−7.94 (m, 1H), 7.91−7.87 (m, 2H), 7.59−7.55 (m, 1H), 7.53 (dd, J = 2.8, 1.4 Hz, 1H), 7.42−7.38 (m, 1H), 7.31 (d, J = 2.2 Hz, 1H), 7.03 (dd, J = 8.3, 1.9 Hz, 1H), 6.91−6.82 (m, 3H), 5.80 (q, J = 6.1 Hz, 1H), 4.47 (tt, J = 7.1, 3.5 Hz, 1H), 3.98 (s, 3H), 3.88−3.68 (m, 2H), 3.37−3.27 (m, 2H), 1.98−1.89 (m, 2H), 1.83−1.71 (m, 5H), 1.46 (s, 9H).

(±)-Methyl 4-(5-(1-Methylpiperidin-4-yloxy)-1*H*-benzo[*d*]imidazol-1-yl)-2-(1-(2-(trifluoromethyl)phenyl)ethoxy)benzoate (*rac*-23c).

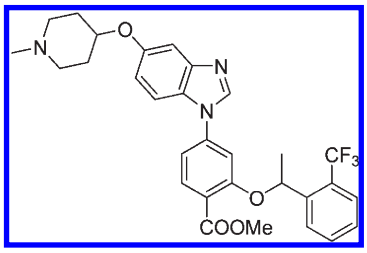

A solution of benzimidazole ***rac*-23a** (205 mg, 0.32 mmol) in DCM (3.4 mL) was treated with trifluoroacetic acid (1.14 mL, 14.7 mmol) at 0 °C. The mixture stirred for 1 h and quenched carefully with aq NaOH solution (2M, 7 mL). To this was added aq sodium bicarbonate solution, and the mixture was extracted with DCM and Et_2O. The combined organic layers were concentrated to afford the crude, unprotected amine ***rac*-25** (170 mg, 98%).

A solution of crude amine ***rac*-25** (87 mg, 0.161 mmol) in DCM (1.8 mL) and MeOH (0.9 mL) was treated with formaldehyde in water (37% w/w, 26 μL, 0.32 mmol) and AcOH (0.011 mL, 0.193 mmol). To this mixture was added sodium triacetoxyborohydride (51 mg, 0.242 mmol), and the reaction mixture stirred for 1 h at room temperature. The reaction was quenched with satd aqueous sodium bicarbonate and the mixture extracted with DCM and EtOAc. The organics were dried (Na_2SO_4) and concentrated to afford benzimidazole ***rac*-23c** (39 mg, 47%). HRMS (ESI) m/z calcd for $C_{30}H_{31}F_3N_3O_4$ (M + H) 554.2261, found 554.2272. ^{1}H NMR (500 MHz, $CDCl_3$) δ 7.96 (d, J = 8.3 Hz, 1H), 7.92−7.89 (m, 2H), 7.70 (d, J = 7.9 Hz, 1H), 7.59 (t, J = 7.6 Hz, 1H), 7.43 (t, J = 7.6 Hz, 1H), 7.31 (d, J = 2.2 Hz, 1H), 7.05 (dd, J = 8.3, 2.2 Hz, 1H), 6.93−6.84 (m, 3H), 5.81 (d, J = 6.2 Hz, 1H), 4.40−4.33 (m, 1H), 4.00 (s, 3H), 2.85−2.72 (m, 2H), 2.39 (d, J = 19.9 Hz, 5H), 2.15−2.06 (m, 2H), 1.97−1.86 (m, 2H), 1.76 (d, J = 6.2 Hz, 3H).

(±)-4-(5-(1-Methylpiperidin-4-yloxy)-1*H*-benzo[*d*]imidazol-1-yl)-2-(1-(2-(trifluoromethyl)phenyl)ethoxy)benzamide (*rac*-24a).

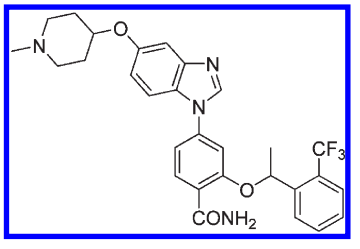

A solution of ester ***rac*-23c** (20 mg, 0.036 mmol) was treated with ammonia in methanol (7M, 4 mL) and heated to 70 °C in a closed-cap vial for 3 days. The mixture was concentrated, and the residue was

purified by Biotage column chromatography (0−100% (DCM/1 M NH_3 in MeOH 9:1)/DCM) to afford amide ***rac*-24a** (18 mg 93%). HRMS (ESI) *m/z* calcd for $C_{29}H_{30}F_3N_4O_3$ (M + H) 539.2265, found 539.2281. ^{1}H NMR (500 MHz, MeOD) δ 8.23 (s, 1H), 8.11 (d, J = 8.3 Hz, 1H), 7.82 (t, J = 7.0 Hz, 2H), 7.70 (t, J = 7.6 Hz, 1H), 7.58 (t, J = 7.6 Hz, 1H), 7.26−7.22 (m, 2H), 6.97 (d, J = 1.9 Hz, 1H), 6.84 (dd, J = 8.9, 2.3 Hz, 1H), 6.66 (d, J = 8.9 Hz, 1H), 5.96 (q, J = 6.1 Hz, 1H), 4.49−4.41 (m, 1H), 2.82−2.74 (m, 2H), 2.49−2.38 (m, 2H), 2.35 (s, 3H), 2.11−2.02 (m, 2H), 1.90−1.80 (m, 5H).

■ ASSOCIATED CONTENT

Supporting Information. Experimental procedures, analytical data for intermediates and final compounds ***rac*-1**, **13a−f**, **19**, (***R*)-24a**, (***S*)-24a**, **24b−d**, a summary of crystallographic analysis of compounds ***rac*-1**, **13f**, **13c**, and ***rac*-24a**, kinase selectivity data for compound ***rac*-24a**, and metabolic data for ***rac*-24a** and (***R*)-24a**. This material is available free of charge via the Internet at http://pubs.acs.org.

Accession Codes

[†]Atomic coordinates and structure factors for the crystal structures of ligand bound Nek2 can be accessed using the following PDB codes: ***rac*-1** (2XNM), **13f** (2XNN), **13c** (2XNO), ***rac*-24a** (2XNP).

■ AUTHOR INFORMATION

Corresponding Author

*For R. B.: phone, +44 20 71535557; e-mail, richard.bayliss@icr.ac.uk. For S.H.: phone, +44 20 87224353; fax, +44 20 87224047; e-mail, swen.hoelder@icr.ac.uk.

Author Contributions

[⊥]These authors contributed equally to this work.

■ ACKNOWLEDGMENT

We acknowledge NHS funding to the NIHR Biomedical Research Centre and funding from Cancer Research UK programme grant number C309/A8274. R.B. acknowledges support from Cancer Research UK (grant C24461/A10285 and infrastructure support for Structural Biology at the ICR), a Royal Society Research Fellowship and the Career Development Programme of the ICR. We are thankful to Prof. Julian Blagg, Prof. Roger Griffin, Dr. Ian Collins, and Prof. Paul Workman for helpful discussions. We also thank Dr. Amin Mirza, Meirion Richards, and Dr. Maggie Liu for their help with HPLC, NMR, and mass spectrometry, Angela Hayes for DMPK analyses, and Maura Westlake and Dr. Lisa Pickard for cellular assays. We are indebted to the staff of DIAMOND beamline I03 and ESRF beamline ID14-2 as well as our many colleagues of the Section of Structural Biology (ICR in London) for their support during data collection.

■ ABBREVIATIONS USED

Abl, Abelson murine leukemia viral oncogene; ADP, adenosine diphosphate; ATP, adenosine triphosphate; Boc, *tert*-butoxycarbonyl; C-Nap1, centrosomal Nek2-associated protein 1; dba, dibenzylideneacetone; DCM, dichloromethane; DMF, *N*,*N*-dimethylformamide; DFG, Asp-Phe-Gly; Hec1, highly expressed in cancer 1; DMSO, dimethyl sulfoxide; HLM, human liver microsomes; HMGA2, high mobility group AT-hook 2; ITC, isothermal titration calorimetry; Lck, lymphocyte-specific protein tyrosine kinase; LE, ligand efficiency; KDR, kinase insert domain receptor; Mad, mitotic arrest deficient-like; MLM, mouse liver microsomes; Nek, NIMA (never in mitosis gene a)-related kinase; Nlp, ninein-like protein; Plk, polo-like kinase; PAMPA, parallel artificial membrane permeability assay; PMB, paramethoxybenzyl; PPTS, pyridinium *p*-toluenesulfonate; SAR, structure−activity relationship; SD, standard deviation; TFA, trifluoroacetic acid; THF, tetrahydrofuran

■ REFERENCES

(1) Jackson, J. R.; Patrick, D. R.; Dar, M. M.; Huang, P. S. Targeted antimitotic therapies: can we improve on tubulin agents?. *Nature Rev. Cancer* **2007**, *7*, 107–117.

(2) (a) Degenhardt, Y.; Lampkin, T. Targeting Polo-like kinase in cancer therapy. *Clin. Cancer Res.* **2010**, *16*, 384–389. (b) Carpinelli, P.; Moll, J. Is there a future for Aurora kinase inhibitors for anticancer therapy? *Curr Opin. Drug Discovery Dev.* **2009**, *12*, 533–542.

(3) O'Regan, L.; Blot, J.; Fry, A. M. Mitotic regulation by NIMA-related kinases. *Cell Div.* **2007**, *2*, 25–36.

(4) Chen, Y.; Riley, D. J.; Zheng, L.; Chen, P. L.; Lee, W. H. Phosphorylation of the mitotic regulator protein Hec1 by Nek2 kinase is essential for faithful chromosome segregation. *J. Biol. Chem.* **2002**, *277*, 49408–49416.

(5) Lou, Y.; Yao, J.; Zereshki, A.; Dou, Z.; Ahmed, K.; Wang, H.; Hu, J.; Wang, Y.; Yao, X. NEK2A interacts with MAD1 and possibly functions as a novel integrator of the spindle checkpoint signaling. *J. Biol. Chem.* **2004**, *279*, 20049–20057.

(6) Hayward, D. G.; Fry, A. M. Nek2 kinase in chromosome instability and cancer. *Cancer Lett.* **2006**, *237*, 155–166.

(7) Emmitte, K. A.; Adjebang, G. M.; Andrews, C. W.; Alberti, J. G.; Bambal, R.; Chamberlain, S. D.; Davis-Ward, R. G.; Dickson, H. D.; Hassler, D. F.; Hornberger, K. R.; Jackson, J. R.; Kuntz, K. W.; Lansing, T. J.; Mook, R. A., Jr.; Nailor, K. E.; Pobanz, M. A.; Smith, S. C.; Sung, C. M.; Cheung, M. Design of potent thiophene inhibitors of polo-like kinase 1 with improved solubility and reduced protein binding. *Bioorg. Med. Chem. Lett.* **2009**, *19*, 1694–1697.

(8) Whelligan, D. K.; Solanki, S.; Taylor, D.; Thomson, D. W.; Cheung, K. M. J.; Boxall, K.; Mas-Droux, C.; Barillari, C.; Burns, S.; Grummitt, C. G.; Collins, I.; van Montfort, R. L. M.; Aherne, G. W.; Bayliss, R.; Hoelder, S. Aminopyrazine inhibitors binding to an unusual inactive conformation of the mitotic kinase Nek2: SAR and structural characterization. *J. Med. Chem.* **2010**, *53*, 7682–7698.

(9) (a) Hornberger, K.; Cheung, M.; Pobanz, M. A.; Emmitte, K. A.; Kuntz, K. W.; Badiang, J. G. Regioselective process for preparing benzimidazole thiophenes. (Smithkline Beecham Corporation). Patent WO2007030366, 2007; (b) Hornberger, K. R.; Badiang, J. G.; Salovich, J. M.; Kuntz, K. W.; Emmitte, K. A.; Cheung, M. Regioselective synthesis of benzimidazole thiophene inhibitors of polo-like kinase 1. *Tetrahedron Lett.* **2008**, *49*, 6348–6351. (c) Hornberger, K. R.; Adjebang, G. M.; Dickson, H. D.; Davis-Ward, R. G. A mild, one-pot synthesis of disubstituted benzimidazoles from 2-nitroanilines. *Tetrahedron Lett.* **2006**, *47*, 5359–5361.

(10) Emmitte, K. A.; Andrews, C. W.; Badiang, J. G.; Davis-Ward, R. G.; Dickson, H. D.; Drewry, D. H.; Emerson, H. K.; Epperly, A. H.; Hassler, D. F.; Knick, V. B.; Kuntz, K. W.; Lansing, T. J.; Linn, J. A.; Mook, R. A., Jr.; Nailor, K. E.; Salovich, J. M.; Spehar, G. M.; Cheung, M. Discovery of thiophene inhibitors of polo-like kinase. *Bioorg. Med. Chem. Lett.* **2009**, *19*, 1018–1021.

(11) (a) Chao, J.; Taveras, A. G.; Aki, C. J. Synthesis of functionalized hydroxy-thiophene motifs as amido- and sulfonamido-phenol bioisosteres. *Tetrahedron Lett.* **2009**, *50*, 5005–5008. (b) Barker, J. M.; Huddleston, P. R.; Wood, M. L.; Burkitt, S. A. Nitration of methyl-3-hydroxy- and 5-methyl-3-hydroxy-thiophene-2-carboxylate, and some chemistry of the products. *J. Chem. Res.* **2001**, *(S)*, 401–402.

(12) Mitsunobu, O. The use of diethyl azodicarboxylate and triphenylphosphine in synthesis and transformation of natural-products. *Synthesis* **1981**, 1–28.

(13) Agback, K. H. Azo-bis-salicylic acid and salt thereof, to treat inflammatory conditions of the intestine. (*Pharmacia AB*). U.S. Patent US4591584, 1986.

(14) Prepared using 1-methylpiperidin-4-ol, 2-bromo-4-fluoro-1-nitrobenzene and sodium hydride in THF at room temperature.

(15) Anilines (***R***)-**16** and (***S***)-**16** were obtained by catalytic reduction under hydrogen atmosphere from the corresponding enantiopure nitroderivatives (see Supporting Information for details).

(16) Compounds ***rac*-24a**, (***R***)-**24a** and (***S***)-**24a** were prepared using the same route described in Schemes 4 and 5. The two enantiomers were obtained from commercially available enantiopure (*S*)- or (*R*)-1-(2-(trifluoromethyl)phenyl)ethanol respectively (purchased from Apollo Scientific, Stockport, UK).

(17) Reynolds, C. H.; Tounge, B. A.; Bembenek, S. D. Ligand binding efficiency: trends, physical basis, and implications. *J. Med. Chem.* **2008**, *51*, 2432−2438 and references therein.

(18) Benzimidazoles: (a) Moriarty, K. J.; Winters, M.; Qiao, L.; Ryan, D.; DesJarlis, R.; Robinson, D.; Cook, B. N.; Kashem, M. A.; Kaplita, P. V.; Liu, L. H.; Farrell, T. M.; Khine, H. H.; King, J.; Pullen, S. S.; Roth, G. P.; Magolda, R.; Takahashi, H. Itk kinase inhibitors: initial efforts to improve the metabolical stability and the cell activity of the benzimidazole lead. *Bioorg. Med. Chem. Lett.* **2008**, *18*, 5537–5540. (b) Mader, M.; de Dios, A.; Shih, C.; Bonjouklian, R.; Li, T. C.; White, W.; de Uralde, B. L.; Sanchez-Martinez, C.; del Prado, M.; Jaramillo, C.; de Diego, J. E.; Cabrejas, L. M. M.; Dominguez, C.; Montero, C.; Shepherd, T.; Dally, R.; Toth, J. E.; Chatterjee, A.; Pleite, S.; Blanco-Urgoiti, J.; Perez, L.; Barberis, M.; Lorite, M. J.; Jambrina, E.; Nevill, C. R.; Lee, P. A.; Schultz, R. C.; Wolos, J. A.; Li, L. C.; Campbell, R. M.; Anderson, B. D. Imidazolyl benzimidazoles and imidazo[4,5-*b*]pyridines as potent p38 alpha MAP kinase inhibitors with excellent in vivo antiinflammatory properties. *Bioorg. Med. Chem. Lett.* **2008**, *18*, 179–183. (c) Wittman, M.; Carboni, J.; Attar, R.; Balasubramanian, B.; Balimane, P; Brassil, P.; Beaulieu, F.; Chang, C.; Clarke, W.; Dell, J.; Eummer, J.; Frennesson, D.; Gottardis, M.; Greer, A.; Hansel, S.; Hurlburt, W.; Jacobson, B.; Krishnananthan, S.; Lee, F. Y.; Li, A.; Lin, T. A.; Liu, P.; Ouellet, C.; Sang, X.; Saulnier, M. G.; Stoffan, K.; Sun, Y.; Velaparthi, U.; Wong, H.; Yang, Z.; Zimmermann, K.; Zoeckler, M.; Vyas, D. Discovery of a 1*H*-(benzoimidazol-2-yl)-1*H*-pyridin-2-one (BMS-536924) inhibitor of insulin-like growth factor I receptor kinase with in vivo antitumor activity. *J. Med. Chem.* **2005**, *48*, 5639–5643. (d) Arienti, K. L.; Brunmark, A.; Axe, F. U.; McClure, K.; Lee, A.; Blevitt, J.; Neff, D. K.; Huang, L.; Crawford, S.; Pandit, C. R.; Karlsson, L.; Breitenbucher, J. G. Checkpoint kinase inhibitors SAR and radioprotective properties of a series of 2-arylbenzimidazoles. *J. Med. Chem.* **2005**, *48*, 1873−1885; purines: (e) Wong, C.; Griffin, R. J.; Hardcastle, I. R.; Northen, J. S.; Wang, L. Z.; Golding, B. T. Synthesis of sulfonamide-based kinase inhibitors from sulfonates by exploiting the abrogated SN_2 reactivity of 2,2,2-trifluoroethoxysulfonates. *Org. Biomol. Chem.* **2010**, *8*, 2457–2464. (f) Huang, W. S.; Zhu, X.; Wang, Y.; Azam, M.; Wen, D.; Sundaramoorthi, R.; Thomas, R. M.; Liu, S.; Banda, G.; Lentini, S. P.; Das, S.; Xu, Q.; Keats, J.; Wang, F.; Wardwell, S.; Ning, Y.; Snodgrass, J. T; Broudy, M. I.; Russian, K.; Daley, G. Q.; Iuliucci, J.; Dalgarno, D. C.; Clackson, T.; Sawyer, T, K.; Shakespeare, W. C. 9-(Arenethenyl)purines as dual Src/Abl kinase inhibitors targeting the inactive conformation: design, synthesis, and biological evaluation. *J. Med. Chem.* **2009**, *52*, 4743–4756. (g) Oumata, N.; Bettayeb, K.; Ferandin, Y.; Demange, L.; Lopez-Giral, A.; Goddard, M. L.; Myrianthopoulos, V.; Mikros, E.; Flajolet, M.; Greengard, P.; Meijer, L.; Galons, H. Roscovitine-derived, dual-specificity inhibitors of cyclin-dependent kinases and casein kinases 1. *J. Med. Chem.* **2008**, *51*, 5229−5242; imidazopyridines: (h) Sato, Y.; Onozaki, Y.; Sugimoto, T.; Kurihara, H.; Kamijo, K.; Kadowaki, C.; Tsujino, T.; Watanabe, A.; Otsuki, S.; Mitsuya, M.; Iida, M.; Haze, K.; Machida, T.; Nakatsuru, Y.; Komatani, H.; Kotani, H.; Iwasawa, Y. Imidazopyridine derivatives as potent and selective polo-like kinase (PLK) inhibitors. *Bioorg. Med. Chem. Lett.* **2009**, *19*, 4673–4678. (i) Hamdouchi, C.; Zhong, B.; Mendoza, J.; Collins, E.; Jaramillo, C.; De Diego, J. E.; Robertson, D.; Spencer, C. D.; Anderson, B. D.; Watkins, S. A.; Zhang, F.; Brooks, H. B. Structure-based design of a new class of highly selective aminoimidazo[1,2-*a*]pyridine-based inhibitors of cyclin dependent kinases. *Bioorg. Med. Chem. Lett.* **2005**, *15*, 1943–1947.

(19) (a) Bembenek, S. D.; Tounge, B. A.; Reynolds, C. H. Ligand efficiency and fragment-based drug discovery. *Drug Discovery Today* **2009**, *14*, 278–283. (b) Ferenczy, G. G.; Keseru, G. M. Enthalpic efficiency of ligand binding. *J. Chem. Inf. Model* **2010**, *50*, 1536–1541.

(20) Reynolds, C. H.; Bembenek, S. D.; Tounge, B. A. The role of molecular size in ligand efficiency. *Bioorg. Med. Chem. Lett.* **2007**, *17*, 4258–4261.

(21) Westwood, I.; Cheary, D. M.; Baxter, J. E.; Richards, M. W.; van Montfort, R. L.; Fry, A. M.; Bayliss, R. Insights into the conformational variability and regulation of human Nek2 kinase. *J. Mol. Biol.* **2009**, *386*, 476–485.

(22) Meyer, E. A.; Castellano, R. K.; Diederich, F. Interactions with aromatic rings in chemical and biological recognition. *Angew. Chem., Int. Ed.* **2003**, *42*, 1210–1250.

(23) Liao, J. J.-L. Molecular recognition of protein kinase binding pockets for design of potent and selective kinase inhibitors. *J. Med. Chem.* **2007**, *50*, 409–424.

(24) Bissantz, C.; Kuhn, B.; Stahl, M. A medicinal chemist's guide to molecular interactions. *J. Med. Chem.* **2010**, *53*, 5061–5084.

(25) Kuntz, I. D.; Chen, K.; Sharp, K. A.; Kollman, P. A. The maximal affinity of ligands. *Proc. Natl. Acad. Sci. U.S.A.* **1999**, *96*, 9997–10002.

(26) Hoffmann, W. W. Allylic 1,3-strain as a controlling factor in stereoselective transformations. *Chem. Rev.* **1989**, *89*, 1841–1860.

(27) Watanabe, M.; Hirokawa, T.; Kobayashi, T.; Yoshida, A.; Ito, Y.; Yamada, S.; Orimoto, N.; Yamasaki, Y.; Arisawa, M.; Shuto, S. Investigation of the bioactive conformation of histamine H_3 receptor antagonists by the cyclopropylic strain-based conformational restriction strategy. *J. Med. Chem.* **2010**, *53*, 3585–3593.

(28) Muley, L.; Baum, B.; Smolinski, M.; Freindorf, M.; Heine, A.; Klebe, G.; Hangauer, D. G. Enhancement of hydrophobic interactions and hydrogen bond strength by cooperativity: synthesis, modeling, and molecular dynamics simulations of a congeneric series of thrombin inhibitors. *J. Med. Chem.* **2010**, *53*, 2126–2135.

(29) Cox, C. D.; Coleman, P. J.; Breslin, M. J.; Whitman, D. B.; Garbaccio, R. M.; Fraley, M. E.; Buser, C. A.; Walsh, E. S.; Hamilton, K.; Schaber, M. D.; Lobell, R. B.; Tao, W.; Davide, J. P.; Diehl, R. E.; Abrams, M. T.; South, V. J.; Huber, H. E.; Torrent, M.; Prueksaritanont, T.; Li, C.; Slaughter, D. E.; Mahan, E.; Fernandez-Metzler, C.; Yan, Y.; Kuo, L. C.; Kohl, N. E.; Hartman, G. D. Kinesin spindle protein (KSP) inhibitors. Discovery of (2*S*)-4-(2,5-Difluorophenyl)-*N*-[(3*R*,4*S*)-3-fluoro-1-methylpiperidin-4-yl]-2-(hydroxymethyl)-*N*-methyl-2-phenyl-2,5-dihydro-1*H*-pyrrole-1-carboxamide (MK-0731) for the treatment of taxane-refractory cancer. *J. Med. Chem.* **2008**, *51*, 4239–4252.

(30) Hayward, D. G.; Newbatt, Y.; Pickard, L.; Byrne, E.; Mao, G.; Burns, S.; Sahota, N. K.; Workman, P.; Collins, I.; Aherne, W.; Fry, A. M. Identification by high-throughput screening of viridin analogs as biochemical and cell-based inhibitors of the cell cycle regulated Nek2 kinase. *J. Biomol. Screening* **2010**, *15*, 918–927.